Physics of semiconductor devices & renewable energies journal

Vol. 01 n. 01 (2023) ; ISSN 2992-040X
Journal homepage: www.psdrej.com

Control of dual star induction generator based on multi-level inverter used in wind energy conversion system

Mohamed Haithem LAZREG [1]*, Hamza MESAI-AHMED [2, 3] and Abderrahim BENTAALLAH [2]

[1] *Laboratoire d'Automatique de Tlemcen (LAT), Université de Tlemcen, Algérie*
[2] *Laboratoire ICEPS, Université Djillali Liabès BP 98 Sidi Bel-Abbès, Algérie*
[3] *CISE - Electromechatronic Systems Research Centre, University of Beira Interior, Covilhã, Portugal*
*Corresponding author *Email: mohamedhaithem.lazreg@univ-tlemcen.dz*

Abstract

This paper presents vector control of dual star induction generator (DSIG) integrated into variable speed wind energy and supplied by three-level NPC converters. Now the DSIG is the most common among multiphase machines when used in high power generation systems, which is associated with two converters. Maximum power point tracking (MPPT) for extracting a maximum of power fluctuating wind speed is illustrated. In order to decrease the fluctuations that appear in the currents generated by DSIG to the electrical network, we propose the NPC structure three-level inverter. Simulation results of a 1.5 MW Wind turbine are presented to illustrate the validity of this application.

Keywords: *Wind Energy; Dual star Induction Generator (DSIG); Maximum Power Point Tracking (MPPT); Field oriented control (FOC); Neutral Point Clamped (NPC) inverter.*

1. Introduction

Due to the environment and global climate change, renewable energy sources play a vital role in the energy market. Among several sources of renewable energy, Wind energy is one of the most important and most promising renewable sources of energy throughout the world in terms of development. Because it is non-polluting and economically viable [1]. Wind energy is carried by the winds. This is indirectly due to solar energy which, by creating temperature differences between hot and cold regions, causes winds. With this mechanical energy, wind turbines can produce electrical energy.

The turbines of last generation operate at variable speed. This type of operation have many advantages such as maximum power operation and higher energy efficiency with low voltage peaks on components and power [2]. In relation to the turbines to fixed speed this are the control algorithms that allow controlling the active and reactive power produced by the wind turbine at each moment in time [3].

In terms of the generators for wind energy conversion system (WECS), we can use several types of electric generators as doubly fed induction generators, permanent magnet synchronous generator or the dual star

induction generator [4,5]. The DSIG has more advantages than conventional cage induction generator, As, high reliability, minimizing torque ripples and segmentation power [6].

The advantages of multi-level converters are well known from the first NPC (Neutral Point Clamped) inverter, which was proposed in 1981 by Nabae et al [7]. The particular topology of the multilevel inverters increases the converted power because the blocking voltage of each switch corresponds to half of

the DC bus voltage [8,9]. In addition, the harmonic content of the modulated voltage is much smaller compared to that of two-level inverters with the same switching frequency [10].

Our contribution to this work will be to propose a way to reduce the resulting fluctuations in currents and to adapt the high power generated, which justifies the use of multilevel converters.

2. Wind turbine model

2.1. Modeling of the Wind Turbine and Gearbox

The available power at a surface S swept by the wind turbine is expressed as follows [11]:

$$P_v = \frac{1}{2}\rho\pi R^2 V^3 \tag{1}$$

Where V is wind speed (m/s), ρ is the density of the air and R is the length of a blade or the radius of the wind turbine (m).

The wind turbine can recover only a fraction of the power of the wind which appears to the rotor of wind turbine, represent by the following expression [12]:

$$P_t = C_p P_v = \frac{1}{2}\rho\pi R^2 V^3 C_P(\lambda,\beta) \tag{2}$$

Where C_p (λ) is the power factor characterizes the aerodynamic efficiency of the turbine (Figure 1). It depends on: the dimensions of the blade, the angle of orientation of the blade β and the ratio of the speed λ. The relative velocity λ is defined as the ratio between the linear speed of the blades ($\Omega_t R$) and the wind speed as follows [13] [14]:

$$\lambda = \frac{\Omega_t R}{V} \tag{3}$$

Where Ω_t (rad/s) is the mechanical speed of the turbine shaft. The torque exerted by the wind on the turbine shaft is defined by:

$$C_t = \frac{P_t}{\Omega_t} = \frac{1}{2}\rho\pi R^3 V^2 C_c(\lambda,\beta) \tag{4}$$

Where C_c represents the torque coefficient:

$$C_c = \frac{C_P}{\lambda} \tag{5}$$

The gearbox conversion ratio (rgb), is designed to match the low-speed turbine blades with the high-speed generator. For a given rated speed of the generator and turbine, the gearbox ratio can be determined by:

$$\Omega_t = \frac{\Omega_g}{G} \tag{6}$$

$$C_g = \frac{C_t}{G} \tag{7}$$

Where Ω_t and Ω_g are the turbine and generator rated speeds in rpm.

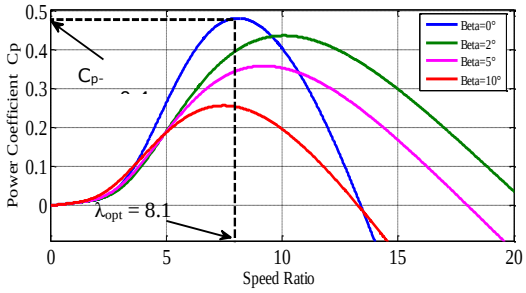

Figure 1. Coefficient of the pair C_p as a function of λ for different β.

2.2. Dual Star Induction Generator Model

The model of dual stator induction machine is composed of a stator with two identical phase windings shifted by an electric angle α = 30°, and a squirrel cage rotor [15, 16]. Under the assumptions of magnetic circuits linearity, and assuming sinusoidal distributed air-gap flux density, the equivalent two-phase model of dual stator induction machine, represented in asynchronous frame (d, q) and expressed in state-space form, is a fourth-order model [17]:

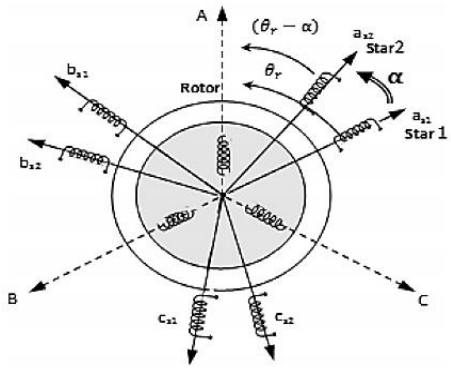

Figure 2. Schematic model of dual stator induction generator.

$$\left[\dot{I}\right] = \left[L^{-1}\right]\left\{[B][U] - \omega_{gl}[C][I] - [D][I]\right\} \tag{8}$$

Where

$$\omega_{gl} = \omega_s - \omega_r \qquad \omega_r = p * \Omega_{mec}$$

$$[U] = \begin{bmatrix} V_{ds1} & V_{qs1} & V_{ds2} & V_{qs1} & V_{dr} & V_{qr} \end{bmatrix}^T$$

$$[I] = \begin{bmatrix} I_{ds1} & I_{qs1} & I_{ds2} & I_{qs1} & I_{dr} & I_{qr} \end{bmatrix}^T$$

$$[B] = diag[1 \quad 1 \quad 1 \quad 1 \quad 0 \quad 0]$$

$$[C] = \begin{bmatrix} 0 & 0 & 0 & 0 & 0 & 0 \\ 0 & 0 & 0 & 0 & 0 & 0 \\ 0 & 0 & 0 & 0 & 0 & 0 \\ 0 & 0 & 0 & 0 & 0 & 0 \\ 0 & -Lm & 0 & -Lm & 0 & -(Lr+Lm) \\ Lm & 0 & Lm & 0 & Lr+Lm & 0 \end{bmatrix}$$

$$[L] = \begin{bmatrix} (Ls1+Lm) & 0 & Lm & 0 & Lm & 0 \\ 0 & (Ls1+Lm) & 0 & Lm & 0 & Lm \\ Lm & 0 & (Ls2+Lm) & 0 & Lm & 0 \\ 0 & Lm & 0 & (Ls2+Lm) & 0 & Lm \\ Lm & 0 & Lm & 0 & (Lr+Lm) & 0 \\ 0 & Lm & 0 & Lm & 0 & (Lr+Lm) \end{bmatrix}$$

$$[D] = \begin{bmatrix} Rs1 & -\omega_s(Ls1+Lm) & 0 & -\omega_s Lm & 0 & -\omega_s Lm \\ \omega_s(Ls1+Lm) & Rs1 & \omega_s Lm & 0 & \omega_s Lm & 0 \\ 0 & -\omega_s Lm & Rs2 & -\omega_s(Ls2+Lm) & 0 & -\omega_s Lm \\ \omega_s Lm & 0 & ws(Ls2+Lm) & Rs2 & \omega_s Lm & 0 \\ 0 & 0 & 0 & 0 & Rr & 0 \\ 0 & 0 & 0 & 0 & 0 & Rr \end{bmatrix}^T$$

The modeling of the mechanical system, can be presented by [18]:

$$J\frac{d\Omega_r}{dt} = T_r - T_{em} - J\Omega_r \tag{9}$$

With T_{em} is the electromagnetic torque, is expressed by:

$$T_{em} = P\frac{Lm}{(Lm+Lr)}\left[\left(i_{qs1}+i_{qs2}\right)\varphi_{dr} - \left(i_{ds1}+i_{ds2}\right)\varphi_{qr}\right] \tag{10}$$

The active and reactive power, are presented by:

$$P_s = V_{ds1}I_{ds1} + V_{qs1}I_{qs1} + V_{ds2}I_{ds2} + V_{qs2}I_{qs2} \tag{11}$$

$$Q_s = V_{qs1}I_{ds1} - V_{ds1}I_{qs1} + V_{qs2}I_{ds2} - V_{ds2}I_{qs2} \tag{12}$$

2.3. Modeling of three-level inverter

The three-level NPC converter of Figure 3 consists of three switching cells connected to a DC bus. Each cell consists of four switches. Since the charge current is alternative, the switches must be antiparallel-mounted transistors with diodes to allow current flow in both directions. Other diodes are used to clamper the terminal of each transistor at the midpoint of the DC bus. If the voltages across the capacitors are kept equal, the compound voltage can be modulated at five voltage levels. In this case, each transistor can support half of the full DC bus voltage in the off state [19].

This structure called neutral point "clamped" is one of the inverter structures with 3-voltage levels. It has a lot of advantage, as the higher number of voltages generated, less harmonic distortion and low switching frequency [20].

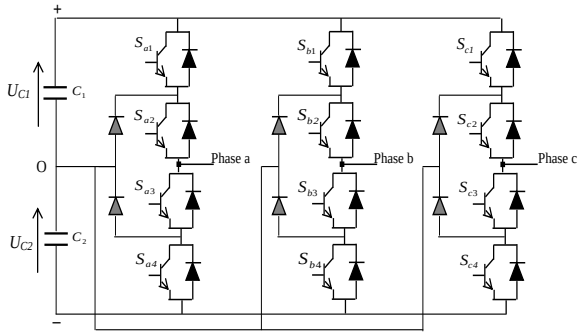

Figure 3. Electrical scheme of a three-level converter - NPC structure.

By combining the four switches (considered perfect) of the same arm, it is possible to impose on phase three levels of different voltages

$$(0,0,1,1) \Rightarrow -\frac{E}{2} = U_{C2}; (0,1,1,0) \Rightarrow 0; (1,1,0,0) \Rightarrow \frac{E}{2} = U_{C1}.$$

With:

The combinations (1,1,1,0) and (0,1,1,1) realize a short circuit of one of the two half sources of DC voltage for which they are prohibited.

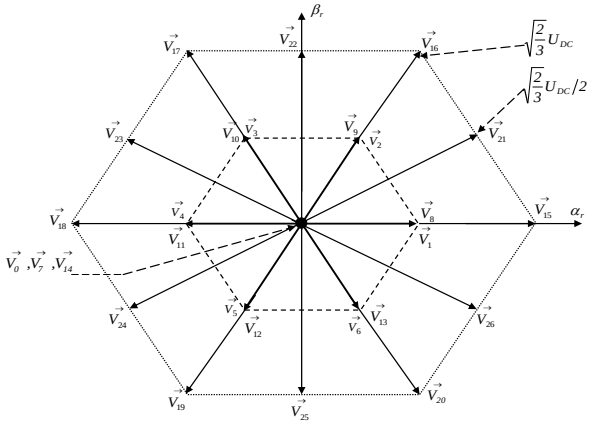

Figure 4. Voltage vectors provided by three level voltages inverter.

Three Boolean command quantities are defined, such as:

$$S_i = -1 \Rightarrow (S_{i1}, S_{i2}, S_{i3}, S_{i4}) = (0,0,1,1)$$
$$S_i = 0 \Rightarrow (S_{i1}, S_{i2}, S_{i3}, S_{i4}) = (0,1,1,0)$$
$$S_i = 1 \Rightarrow (S_{i1}, S_{i2}, S_{i3}, S_{i4}) = (1,1,0,0)$$

As a result, and unlike the 2-level inverter which can only provide eight voltage vectors, including two nulls. the 3-level inverter can produce 27 voltage vectors including three nulls (Figure 4) [9,19].

From the voltage vectors schematized in figure 4 four groups of the vectors can be distinguished:

1. group of vectors "zero tension": They are obtained by three different combinations of the states of the 3 arms: (1,1,1), (-1, -1, -1) and (0,0,0) , and named V_7, V_{14} and V_0, respectively. They have no influence on the voltage of the midpoint of the inverter.

2. group of the vectors "half tension": one can decompose this group into 2 other subgroups:

- The first consists of named vectors: V_1, V_2, V_3, V_4, V_5 and V_6.
- The other consists of vectors: V_8, V_9, V_{10}, V_{11}, V_{12} and V_{13}.

3. group of the "full voltage" vectors: This group contains the vectors of the tensions named V_{15}, V_{16}, V_{17}, V_{18}, V_{19} and V_{20}.

4. The group of vectors "intermediate voltage": the vectors of the tensions of this group are V_{21}, V_{22}, V_{23}, V_{24}, V_{25} and V_{26}.

3. Field oriented control of DSIG:

3.1. Reference frame:

In order to find a variable speed drive where the flux and the electromagnetic torque will be connected directly to the stator current components. We choose a rotor field-oriented control whose the rotor flux is lined up with the d-axis [18] [21].

$$\varphi_{dr} = \varphi_r \tag{13}$$

$$\varphi_{qr} = 0 \tag{14}$$

The DSIG control guideline is like the notable rotor FOC utilized for the IG.

3.2. Control strategy

By applying the self-condition of FOC to equation (9) and (12), the final expressions of slip speed and electromagnetic torque are:

$$T_{em}^{*} = P\frac{Lm}{(Lm+Lr)}\left[\left(i_{qs1}^{*}+i_{qs2}^{*}\right)\varphi_r^{*}\right] \tag{15}$$

$$\omega_{gl}^{*} = \frac{r_r Lm}{(Lm+Lr)}\frac{\left(i_{qs1}^{*}+i_{qs2}^{*}\right)}{\varphi_r^{*}} \tag{16}$$

With $i_{ds1}^{*}+i_{ds2}^{*} = \dfrac{\varphi_r^{*}}{L_m}$ (17)

The references stator voltages are expressed by:

$$V_{ds1}^{*} = R_s i_{ds1} + Ls\frac{di_{ds1}}{dt} - \omega_s^{*}(L_s i_{qs1} + T_r\varphi_r^{*}\omega_{gl}^{*}) \tag{18}$$

$$V_{qs1}^{*} = R_s i_{qs1} + Ls\frac{di_{qs1}}{dt} - \omega_s^{*}(L_s i_{ds1} + \varphi_r^{*}) \tag{19}$$

$$V_{ds2}^{*} = R_s i_{ds2} + Ls\frac{di_{ds2}}{dt} - \omega_s^{*}(L_s i_{qs2} + T_r \varphi_r^{*} \omega_{gl}^{*}) \quad (20)$$

$$V_{qs2}^{*} = R_s i_{qs2} + Ls\frac{di_{qs2}}{dt} - \omega_s^{*}(L_s i_{ds2} + \varphi_r^{*}) \quad (21)$$

Where $T_r = \frac{L_r}{R_r}$

4. Simulation results and discussion

The simulation results of the control system presented in this paper, are implemented using Matlab /Simulink software for the wind speed profile indicated in Figure 5. The DSIG used in this work is limited at 1.5 MW, whose rated parameters are shown in appendix.

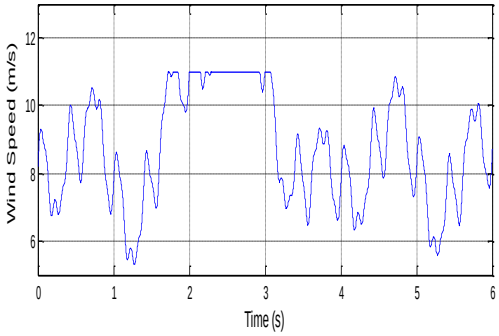

Figure 5. Profile of wind speed

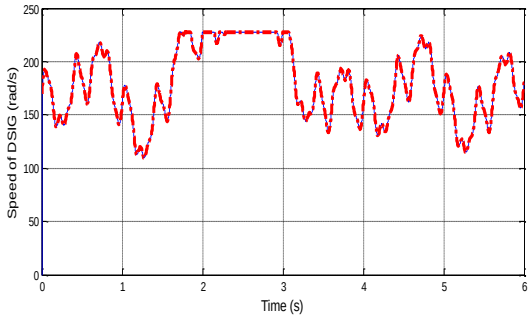

Figure 6. DSIG speed and its reference

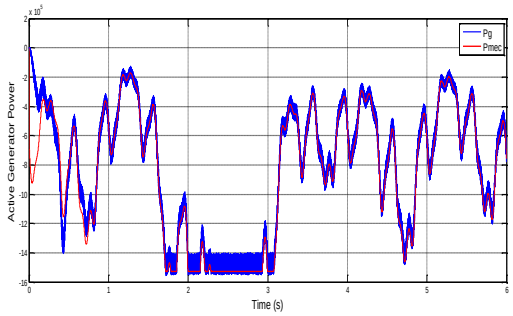

Figure 7. Stator active power (W)

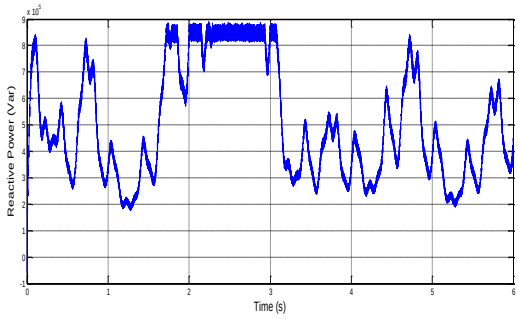

Figure 8. Stator reactive power (Var)

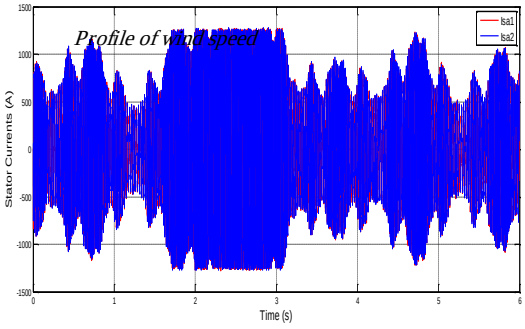

Figure 9. Stator current of star 1 and star 2

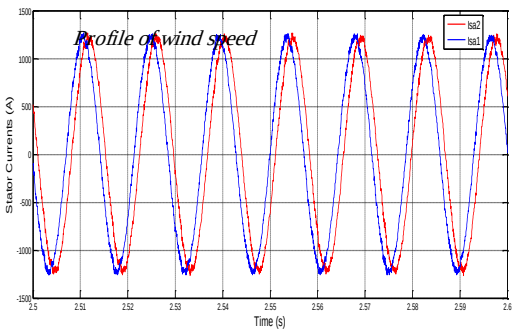

Figure 10. Zoom of Stator current of star 1 and 2

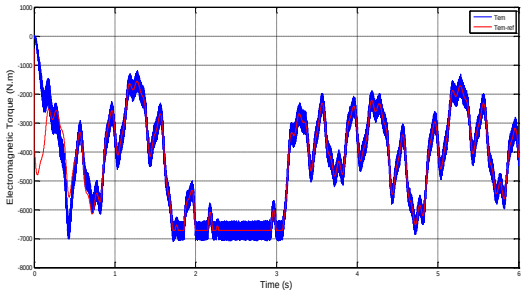

Figure 11. Electromagnetic Torque and its reference

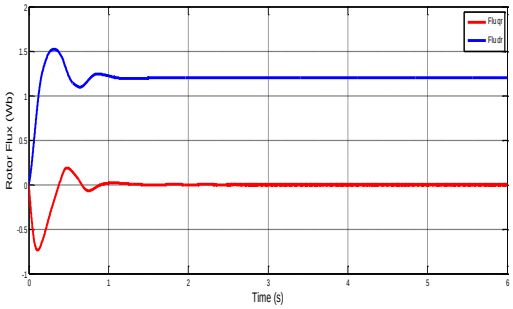

Figure 12. Direct and quadratic Rotor Flux

Profile of wind speed

Profile of wind speed

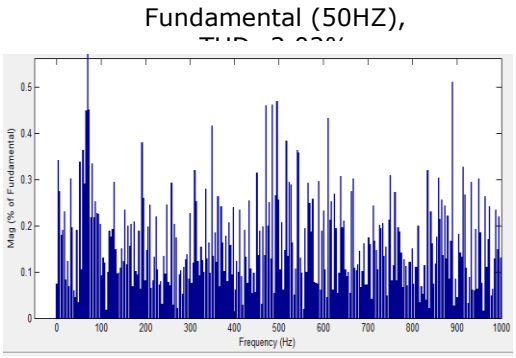

Figure 13. THD spectrum analysis with 2 level

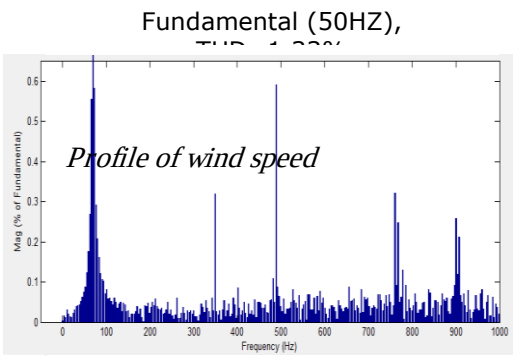

Figure 14. THD spectrum analysis with 3 level

THD spectrum analysis of the grid current ig1

Profile of wind speed

Profile of wind speed

THD spectrum analysis of the grid current ig1

Profile of wind speed

Profile of wind speed

From Figure 6 it is clear that the rotation turbine speed follows perfectly its reference, which varies according on the imposed wind profile.

Figure 9 shows the evolution of DSIG stator currents for the first phase of each star. Their evolution over the entire simulation time is illustrated in Figure 9 and his zoom between 2.5 and 2.6 are shown in Figure 10. These are sinusoidal shifted by 30°.

The waveform of the electromagnetic torque generator follows its desired reference coming from the MPPT control as shown in Figure 11.

The direct and quadratic rotor fluxes of the DSIG are illustrated in Figure 12. They are decoupled, where The component of the direct rotor flux pursues its reference, and the component of the quadratic rotor flux is null.

5. Conclusion

This article has been dedicated to the modeling and synthesis of the control laws of a DSIG - based wind energy conversion system. The study deals only with the aerogenerator-side part, consisting of the aerodynamics of the turbine and its MPPT control, the DSIG and the DC/AC converter.

Characteristics study's of the output voltage of 3L-NPC inverter shown that it has low harmonics. The Vector modulation strategy used to control this inverter using two bipolar carriers allows to widen the setting linear zone of output voltage of the inverter by 15 %.

The control of the DSIG fed by 3L-NPC inverter gave good dynamic performances; this inverter opens an interesting field when used in the high power systems such as electric traction. Future work will address the high-level converter design for DSIG-based WECS for an enhancement of the power quality

Table 1: Appendix parameters

Turbine				
R (m)	Number of blades	G	C_{pmax}	λ_{opt}

	35.25		3		90	0.48	8.01
			DSIG				
P_n (MW)	U_s (V)	F (Hz)	Pair poles	I_n (A)	U_{dc} (V)	
1.5	400	50	2	2000	1130	
R_{s1}, R_{s2} (Ω)	R_r (Ω)	L_{s1}, L_{s2} (H)	L_r (H)	L_m (H)	J (kg.m2)	
0.008	0.007	1.34e-4	6.7e-5	0.0045	1000	

Table 2: Abbreviations and Acronyms

P_s Q_s	Active and réactive Power	**L_{s1}, L_{s2}**	Stator inductances
DSIG	Dual Star Induction Generator	**$V_{ds1.2}$,$V_{qs1.2}$**	d-q stator voltages
MPPT	Maximum Power Pointe Tracking	**I_{ds} I_{qs}**	d-q stator currents
FOC	Field Oriented Control	**I_{dr} I_{qr}**	d-q rotor currents
L_m	Magnetizing inductance	Rr	Rotor resistance
ω_s	Synchronous reference Speed	Rs1, Rs2	Stator resistances
ω_{gl}	Rotor electrical angular speed	Lr	Rotor inductance

References

1. Bu, F.; Hu, Y.; Huang, W. S. Wide-Speed-Range-Operation Dual Stator-Winding Induction Generator DC Generating System for Wind Power Applications. *IEEE Transactions on Power Electronics* **2015**, *vol. 30*, no. 2, pp. 561-573.

2. Achouri, F.; Mendil, B. Wind speed forecasting techniques for maximum power point tracking control in variable speed wind turbine generator. *International Journal of Modelling and Simulation* **2019**, *vol. 39*, no. 4, pp. 246-255.

3. Chekkal, S.; Lahaçani, N.; Aouzellag, D.; Ghedamsi, K. Fuzzy logic control strategy of wind generator based on the dual-stator induction generator. *International Journal of Electrical Power & Energy Systems* **2014**, *vol. 59*, pp. 166-175.

4. Benakcha, M.; Benalia, L.; Ammar, A.; Bourek, A.; Wind energy conversion system based on dual stator induction generator controlled by nonlinear backstepping and pi controllers. *International Journal of System Assurance Engineering and Management* **2018**, *vol. 10*, no. 4, pp. 499-509.

5. Nounou, K.; Marouani, K.; Benbouzid M.; Tabbache, B. DC Bus Voltage Control of a Power Generation System Based on a Dual Star Induction Generator, *International Review of Electrical Engineering (IREE)* **2016**, *vol. 11*, no. 6, p. 686.

6. Chatterjee S.; Chatterjee, S. A novel speed sensor-less vector control of Dual Stator Induction machine with space vector based advanced 9-zone hybrid PWM for grid connected wind energy generation system. *Electric Power Systems Research* **2018**, *vol. 163*, pp. 174-195.

7. Nabae, I.; Takahashi H. A New Neutral-Point-Clamped PWM Inverter. *IEEE Transactions on Industry Applications* **1981**, *vol. -17*, no. 5, pp. 518-523.

8. Baghli, L.; Delpha, D.; Hallouche; Mba,W. Three-Level NPC Inverter Incipient Fault Detection and Classification using Output Current Statistical Analysis. *Energies* **2019**, *vol. 12*, no. 7, p. 1372.

9. Ghennam, T.; Berkouk E.; Francois, B. A Novel Space-Vector Current Control Based on Circular Hysteresis Areas of a Three-Phase Neutral-Point-Clamped Inverter. *IEEE Transactions on Industrial Electronics* **2010**, *vol. 57*, no. 8, pp. 2669-2678.

10. Zhang, Z.; Li, Z.; Kazmierkowski, M.; Rodriguez J.; Kennel, R. Robust Predictive Control of Three-Level NPC Back-to-Back Power Converter PMSG Wind Turbine Systems With Revised Predictions. *IEEE Transactions on Power Electronics* **2018**, *vol. 33*, no. 11, pp. 9588-9598.

11. Tahir, K.; Belfedal, C.; Allaoui T.; Doumi, M. Proposal of a new hybrid control strategy for dynamic performance improvement of wound field synchronous generator-based wind turbines. *Journal of Renewable and Sustainable Energy* **2015**, *vol. 7*, no. 4, p. 043113.

12. Aouzellag, D.; Ghedamsi K.; Berkouk, E.; Network power flux control of a wind generator. *Renewable Energy* **2009**, *vol. 34*, no. 3, pp. 615-622.

13. Kouzou, A. Identification and Modeling of Wind Turbine Variables for Efficient Energetic Conversion. 15th International Multi-Conference on Systems, Signals & Devices (SSD), 2018.

14. Yasmine Ihedrane, Chakib El Bekkali, BadreBossoufi. Direct and indirect field oriented control of DFIG-generators for wind turbines variable-speed. 14th International Multi-Conference on Systems, Signals & Devices (SSD), 2017.

15. Ameur F, Kouzi K, Ameur A, Kasbadji NM. Robust control of dual stator induction generator used in wind conversion system connectes to the grid usin direct torque control. 4th International conference on renewable energy: generation and applications ICREGA'16, At Belfort, French, 2016.

16. Khlifi, M. Behavior of a Dual Stator Induction Machine Fed by Neutral Point Clamped Multilevel Inverter. *Journal of Energy* **2018**, *vol. 2018*, pp. 1-10.
17. Ameur, F.; Kouzi, K.; Optimized PI and Fuzzy Speed Vector Control of Dual Stator Induction Generator Used in a Variable Speed Wind. *International Journal of Electrical Energy* **2014**, pp. 74-81.
18. Tir, Z.; Soufi, Y.; Hashemnia, M.; Malik O.; Marouani, K. Fuzzy logic field-oriented control of double star induction motor drive. *Electrical Engineering* **2016**, *vol. 99*, no. 2, pp. 495-503.
19. Djeriri, Y.; Meroufel, A.; Belabbes B.; Massoum, A. Three-level NPC voltage source converter based direct power control of the doubly fed induction generator at low constant switching frequency. *Revue des Energies Renouvelables, Centre de Développement des Energies Renouvelables- CDER* **2013**, *Vol.16*, No.1, pp.91-103.
20. Ghennam T.; Berkouk, E. Back-to-back three-level converter controlled by a novel space-vector hysteresis current control for wind conversion systems. *Electric Power Systems Research* **2010**, *vol. 80*, no. 4, pp. 444-455.
21. Amimeur, H.; Aouzellag, D.; Abdessemed R.; Ghedamsi, K. Sliding mode control of a dual-stator induction generator for wind energy conversion systems. *International Journal of Electrical Power & Energy Systems* **2012**, *vol. 42*, no. 1, pp. 60-70.